Optimal Placement of Dynamic Energy Storage with Integrated Demand Response: A Multi-Objective Framework for Technical Performance, Safe Operation, and Social Welfare

Mohammadreza Mousavi Khademi[1,*] and Mehdi Zareian Jahromi[2]

[1] *Department of Electrical Engineering, Hormozgan Distribution Electric Company, Iran*
[2] *Department of Electrical Engineering, National Kaohsiung University of Science and Technology (NKUST), Kaohsiung, Taiwan*
** Corresponding author: mousavi.sure@gmail.com*

Manuscript received 11 January, 2026; revised 4 September, 2026; accepted 10 November, 2026. Paper no. JEMT-2607-1609

Modern power systems with high renewable penetration, electrification, and real-time pricing require synchronized supply- and demand-side flexibility. This work develops a two-stage framework for the joint placement and sizing of dynamic energy storage (DES) and the operational coordination of dynamic demand-side management (DSM) as a multi-objective problem balancing technical performance, a safe operating index (SOI), and a social welfare index (SWI). The SWI represents partial-equilibrium consumer utility net of operating and storage-degradation costs, while the SOI combines normalized steady-state voltage-security headroom and expected energy not served (EENS). An online scheduling layer co-optimizes DES dispatch and DSM modulation through hourly receding-horizon updates under uncertainty. In this work, "dynamic" denotes time-coupled hourly scheduling and state-of-charge evolution rather than electromagnetic, electrochemical, or sub-second transient dynamics. The contribution is formulation-level integration of planning and operation, rather than a new generic optimization algorithm. Reference-case validation on the IEEE 69-bus radial distribution feeder shows improvements over controlled reference-informed benchmark configurations in voltage-security headroom, EENS, feeder losses, peak demand, and welfare. The two-stage formulation separates the mixed-integer planning task from the hourly operational update and provides a transparent basis for Pareto trade-off analysis within the evaluated feeder and assumptions. A separate reconstruction-based robustness assessment uses a fixed 10-scenario ensemble and an IEEE 33-bus execution check to quantify dispersion, parameter sensitivity, and scheduling feasibility without extending the claims beyond the evaluated assumptions.

Keywords: *Dynamic energy storage placement, Demand response (real-time pricing), Social welfare index, Safe operating index.*

http://dx.doi.org10.22109/jemt.2026.592289.1609

Nomenclature

Symbol	Definition	Unit/domain
$\mathcal{N},\ i, j$	Bus set and bus indices	dimensionless
$\mathcal{L},\ (i,j)$	Line set and branch indices	dimensionless
$\mathcal{G},\ g$	Generator set and index	dimensionless
$\mathcal{S},\ s$	Candidate DES-site set and index	dimensionless
$\mathcal{T},\ t,\ \Delta t$	Time-period set, index, and interval	h
$\Omega,\ \omega,\ \pi_\omega$	Scenario set, scenario index, and probability	dimensionless
$\hat{d}_{i,t,\omega},\ \hat{q}_{i,t,\omega}$	Baseline active and reactive demand	kW, kvar
$\hat{p}^{r}_{i,t,\omega}$	Available renewable active-power injection	kW
$G_{ij},\ B_{ij}$	Real and imaginary parts of network admittance	p.u.
$V^{min},\ V^{max},\ V_i^{ref}$	Voltage limits and nominal/reference voltage	p.u.
$\bar{F}_{ij},\ \bar{P}_g,\ \bar{Q}_g$	Branch-flow and generator limits	kW, kvar
$\bar{P}_s,\ \bar{E}_s,\ \eta_s^{ch},\ \eta_s^{dis}$	DES power/energy limits and charge/discharge efficiencies	kW, kWh, dimensionless
$\bar{u}_{i,t},\ R_i$	DSM bound and optional energy-neutrality budget	kW, kWh
$\alpha,\ \beta_V,\ w_k$	SOI, voltage-deviation, and objective weights	dimensionless
$h^{ref},\ EENS^{ref}$	Reference scales for security-headroom and adequacy normalization	p.u., MWh

$\lambda_t^0,\ \epsilon_i,\ a_{i,t},\ b_{i,t}$	Reference price, short-run price elasticity, and quadratic-utility coefficients	currency/kWh, dimensionless, model units
$z_s,\ E_s,\ P_s$	First-stage DES placement, energy rating, and power rating	binary, kWh, kW
$p_{g,t,\omega},\ q_{g,t,\omega},\ V_{i,t,\omega},\ \theta_{i,t,\omega}$	Generator outputs, bus-voltage magnitude, and angle	kW, kvar, p.u., rad
$F_{ij,t,\omega},\ p_{s,t,\omega}^{ch},\ p_{s,t,\omega}^{dis}$	Branch flow and DES charge/discharge powers	kW
$SoC_{s,t,\omega},\ u_{i,t,\omega},\ d_{i,t,\omega},\ ls_{i,t,\omega}$	State of charge, DSM adjustment, realized demand, and involuntary curtailment	kWh, kW
$h_{t,\omega},\ ENS_\omega,\ EENS$	Voltage-security headroom, scenario ENS, and expected ENS	p.u., MWh
$U_{i,t}(\cdot),\ C_g(\cdot),\ C_s^{deg}(\cdot)$	Consumer utility, generation cost, and DES degradation cost	currency
$SWI,\ SOI,\ T_{tech},\ TI$	Social-welfare, safe-operation, technical-penalty, and technical indices	normalized/defined in text

1. Introduction

Modern power systems are becoming more variable because of renewable generation, electrification, and loads that respond to prices. This variability increases stress on network limits and can reduce operating margins. Energy storage and demand response provide complementary sources of flexibility, but prior studies often emphasize either planning or operation, use security measures separately from welfare objectives, or do not link storage siting to subsequent price-responsive operation. This paper therefore co-optimizes DES siting/sizing and DSM operation in a two-stage framework. The proposed SOI combines normalized steady-state voltage-security headroom with EENS, while the SWI represents partial-equilibrium consumer utility net of operating and storage-degradation costs. Throughout this paper, dynamic operation means hourly, time-coupled receding-horizon scheduling; it does not denote sub-second transient control. Recent studies since 2022 have favoured coordinated flexibility management on both the storage and demand sides, but important distinctions remain between operational scheduling, asset siting, security assessment, and welfare modeling. Zhang et al. jointly scheduled BESS and demand response to reduce distribution-system operating cost under high renewable penetration [1]. Su et al. addressed storage placement and capacity sizing and demonstrated voltage-profile benefits [2]. Apribowo et al. linked BESS placement to renewable penetration while considering demand-response flexibility [3], and Asadi et al. coordinated storage, switching, and demand response to improve distribution-network reliability [4]. These works establish that storage and flexible demand can be technically and economically complementary. Security-oriented planning has also incorporated voltage-stability constraints [5], while welfare-focused demand-response studies quantify consumer and system benefits [6]. Stability and welfare have been considered through grid-side flexibility devices [7], and two-level coordination has been investigated for power systems and data-center demand under uncertainty [8]. The remaining gap addressed here is therefore narrower than the general co-optimization of storage and demand response: it is the explicit coupling of storage siting/sizing to subsequent hourly DES-DSM recourse while evaluating technical performance, a composite voltage-headroom/EENS safety index, and a price-responsive welfare index under a common set of network constraints. Complementary studies [9]–[13] illustrate related placement, sizing, compensation, and hybrid-resource design strands. Reference [9] coordinates distributed generation and shunt-capacitor placement for loss and cost reduction; [10] derives an analytical economic rule for storage location and capacity; [11] optimizes DG and DSTATCOM placement for loss, voltage-profile, and investment objectives; and [12], [13] address cost-reliability trade-offs in hybrid renewable-storage systems. These studies are relevant to the broader placement literature, but they are not treated here as direct substitutes for a feeder-level planning-operation framework with price-responsive DSM. More recent work provides stronger points of comparison. Zakernezhad et al. developed two-level day-ahead and real-time scheduling of distributed resources, demand-response aggregators, and electrical storage [18]. Najafi-Ghalelou et al. formulated a two-stage, scenario-based social-welfare model for a battery-enabled distribution market with AC-network constraints [19]. Zarei et al. combined multi-objective AC-OPF, demand response, uncertainty, and optimal storage allocation with explicit voltage-variation objectives [20]. These contributions substantially overlap with individual elements of the present formulation and are therefore acknowledged explicitly in positioning the contribution. Market and behavioral studies further emphasize the value of price-responsive demand. Real-time and dynamic pricing can improve economic efficiency and influence consumption, while multi-objective operational formulations expose trade-offs among cost, resilience, and voltage-related performance [14]–[17]. Taken together with [18]–[20], the literature shows that storage, demand response, uncertainty, voltage performance, and welfare have each been treated in sophisticated combinations. The contribution of the present study is not that these ingredients are individually new; rather, the paper places them in one scope-bounded two-stage formulation in which first-stage DES siting/sizing decisions are fixed before uncertainty and second-stage DES-DSM recourse is evaluated using the same technical, safety, and welfare definitions.

Accordingly, this paper makes three formulation-level contributions. First, it explicitly links offline DES siting and sizing to an hourly receding-horizon DES-DSM operating layer under the same network and device constraints. Second, it uses a composite SOI that combines normalized steady-state voltage-security headroom and EENS so that voltage-security and adequacy information can be examined within one operator-selected index. Third, it formulates an SWI for instantaneous-price-responsive demand using consumer utility and real resource costs within a stated partial-equilibrium boundary. Pareto analysis is then used to expose the trade-offs among technical performance, SOI, and SWI. Claims of superiority are restricted to the controlled reference-informed benchmark configurations, IEEE 69-bus feeder, input profiles, and assumptions reported in this study. The central distinction is the coupling of two decision time scales. The planning stage determines DES locations and ratings before uncertainty is realized, whereas the operational stage fixes those investment decisions and coordinates DES dispatch and DSM through a receding-horizon controller. The resulting contribution is an integrated planning-operation formulation, not a claim of a fundamentally new optimization algorithm. Table 1 summarizes the modeled capabilities explicitly reported by representative studies, including the recent overlapping formulations in [18]–[20]. It is a comparison of modeling scope rather than scientific quality. Prior work provides substantial contributions in real-time scheduling, social-welfare maximization, storage allocation, voltage-oriented optimization, reliability, and resilience; however, the specific combination evaluated here couples DES siting with hourly DES-DSM recourse while using the stated SWI and composite SOI under a common network model. The comparison is therefore scope-bounded and does not imply that this formulation is the only possible architecture or that its ranking generalizes to other networks or market assumptions.

Table 1. Comparison of representative studies and the proposed method in terms of modeled features and addressed objectives.

Study	Real-time management/control	Social welfare index under instantaneous pricing (utility + operating cost)	New safe operating index (voltage-security headroom + EENS)	Explicit voltage-security metric	Explicit EENS	Multi-objective across technical, SOI, SWI
[1]	~	—	—	—	—	—
[2]	—	—	—	~ (voltage profile)	—	~ (tech only)
[3]	—	—	—	~	—	~
[4]	~	—	—	—	~ (reliability indices, not EENS)	~
[5]	—	—	—	✓	—	~ (security–cost)
[6]	—	✓ (welfare during DR)	—	—	—	~ (economic objective)
[7]	—	~ (welfare notion)	—	✓ (stability enhancement)	—	~
[8]	~	—	—	—	—	~
[14]	—	✓ (RTP welfare)	—	—	—	—
[15]	—	~ (behavioral welfare implications)	—	—	—	—
[16]	—	—	—	✓ (static stability)	—	✓ (econ–stability)
[17]	—	—	—	~	~	✓ (resilience–econ)
[18]	✓ (DA/RT)	—	—	~ (network limits)	—	~ (robust sched.)
[19]	~ (market)	✓ (SW)	—	~ (AC limits)	—	~ (SW/robust)
[20]	~ (operation)	—	—	✓ (voltage obj.)	—	✓ (cost/peak/V)
Current study	✓	✓	✓	✓	✓	✓

Note: ✓ denotes explicit inclusion of the listed feature, ~ denotes partial or closely related inclusion, and — denotes that the feature is not explicitly modeled under the cited study's reported scope. The table compares modeling scope only; it is not a quality ranking.

The rest of the paper is organized as follows. Section II formalizes the network, DES, DSM, SWI, SOI, and technical-performance models. Section III presents the two-stage multi-objective co-optimization and receding-horizon linkage. Section IV reports the IEEE 69-bus numerical results and controlled benchmark comparisons. Section V concludes the paper and states the principal modeling and validation limitations.

2. Methodology

The proposed method jointly optimizes the placement and sizing of DES with the hourly coordination of DSM under instantaneous price signals. Conceptually (Figure 1), an investment layer chooses storage locations and power/energy ratings, while an operational layer executes a receding-horizon schedule that co-controls storage charging/discharging and price-responsive demand. The term dynamic refers to intertemporal state-of-charge coupling and repeated hourly set-point updates. It does not imply electromagnetic or electrochemical transient modeling. The three co-primary objectives are technical performance, SOI, and SWI, all evaluated under the stated AC-network, device, and scenario constraints.

Figure 1 shows the information flow among the local demand-response controllers, generation and renewable resources, DES units, the main control center, and the multi-objective decision layer. Measurements and demand-response states are sent to the central controller, and coordinated DES and DSM set-points are returned while network, security, and welfare constraints are enforced. The DES locations and ratings are selected in the planning stage and remain fixed during each online operating horizon.

$$\mathrm{SWI} = \sum_{\omega\in\Omega} \pi_\omega \Big(\sum_{t\in T}\sum_{i\in N} U_{i,t}\left(d^{f}_{i,t,\omega}\right) - \sum_{t\in T}\sum_{g\in G} C_g\left(p_{g,t,\omega}\right) - \sum_{t\in T}\sum_{s\in S} C^{\deg}_{s}\left(p^{\mathrm{ch}}_{s,t,\omega}, p^{\mathrm{dis}}_{s,t,\omega}\right)\Big) \tag{1}$$

The SWI is a partial-equilibrium economic-surplus measure, not a Cobb–Douglas or CES model. A concave quadratic utility $U_{i,t}(d) = a_{i,t}d - \frac{1}{2}b_{i,t}d^2$, with $a_{i,t}, b_{i,t} > 0$, represents customer value and is calibrated to price responsiveness; its marginal utility is balanced against operating and degradation costs. Energy payments are transfers and are not double counted in social welfare.

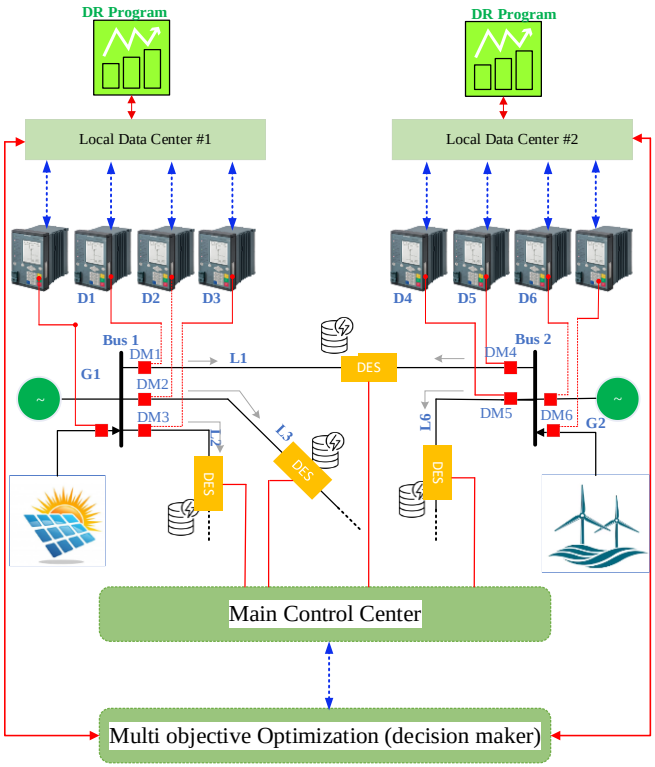

Fig. 1. Conceptual framework of DES placement and demand-side management.

The welfare boundary includes consumers and the supplying system represented in the optimization; consequently, internal energy payments are treated as transfers and are not counted a second time as a social cost. Generation/import resource costs and DES degradation costs remain real costs in the welfare calculation. Thus, SWI is a system-level partial-equilibrium surplus measure, not a customer-bill metric.

For the selected short-run own-price elasticity, the quadratic-utility coefficients are calibrated from baseline demand and the reference price so that marginal utility equals the reference price at the baseline operating point and the local demand slope reproduces the prescribed elasticity:

$$b_{i,t} = -\frac{\lambda_t^0}{\epsilon_i d_{i,t}^f}, \qquad a_{i,t} = \lambda_t^0 + b_{i,t} d_{i,t}^f, \qquad \epsilon_i < 0 \quad (2)$$

Safe operating index, with $\alpha \in [0,1]$ and positive reference scales $h^{\mathrm{ref}}, EENS^{\mathrm{ref}} > 0$:

$$\mathrm{SOI} = \alpha H_V + (1-\alpha) H_E \quad (3)$$

The first SOI component is a steady-state voltage-security headroom, not a transient VSM. The dimensionless components are $H_V = \mathbb{E}_{\omega,t}[h_{t,\omega}/h^{\mathrm{ref}}]$ and $H_E = 1 - EENS/EENS^{\mathrm{ref}}$. They are aggregated over the same scenario and operating horizon before weighting. The coefficient α reflects the operator's security-versus-adequacy preference; sweeping α or applying the epsilon-constraint formulation prevents a single weighting choice from being treated as universal. The reference scales are fixed before optimization and are common to the proposed method and all controlled benchmark configurations. They convert voltage headroom and EENS to dimensionless quantities before aggregation, avoiding a direct combination of p.u. and MWh. The coefficient α is therefore interpreted only as an operator preference between normalized security and adequacy components, not as a physical conversion factor. Any numerical conclusion based on a particular α must remain conditional on the evaluated sensitivity range. The SOI is a transparent composite performance index rather than a probabilistic tail-risk measure; VaR/CVaR-type adequacy terms can be substituted in extensions where explicit tail-risk optimization is required.

Technical-performance penalty based on feeder losses and voltage deviations:

$$T_{\mathrm{tech}} = \sum_{\omega\in\Omega} \pi_\omega \sum_{t\in\mathcal{T}} \left(P_{t,\omega}^{\mathrm{loss}} + \beta_V \sum_{i\in\mathcal{N}} (V_{i,t,\omega} - V_i^{\mathrm{ref}})^2 \right) \quad (4)$$

Here $P_{t,\omega}^{\mathrm{loss}}$ is the total real-power loss computed from branch flows or admittance relations. For presentation in Figures 6 and Table 3, the higher-is-better technical index is $TI = 1 - T_{\mathrm{tech}}^N$, where the superscript N denotes min–max normalization using common ideal and nadir values.

Dimensionless multi-objective scalarization, with $w_k \geq 0$ and $\sum_{k=1}^3 w_k = 1$:

$$\max J = w_1 \mathrm{SWI}^N + w_2 \mathrm{SOI} + w_3 TI \quad (5)$$

AC nodal power balance at each bus i, with $\theta_{ij,t,\omega} = \theta_{i,t,\omega} - \theta_{j,t,\omega}$ and $\mathcal{G}_i, \mathcal{S}_i$ denoting the generators and storage units connected to bus i:

$$\sum_{g\in\mathcal{G}_i} p_{g,t,\omega} + p_{i,t,\omega}^{r,f} + \sum_{s\in\mathcal{S}_i} \left(p_{s,t,\omega}^{\mathrm{dis}} - p_{s,t,\omega}^{\mathrm{ch}} \right) - d_{i,t,\omega} + ls_{i,t,\omega}$$
$$- V_{i,t,\omega} \sum_{j\in\mathcal{N}} V_{j,t,\omega} \left(G_{ij} \cos\theta_{ij,t,\omega} + B_{ij} \sin\theta_{ij,t,\omega} \right) = 0 \quad (6)$$

$$\sum_{g\in\mathcal{G}_i} q_{g,t,\omega} - q_{i,t,\omega}^f = V_{i,t,\omega} \sum_{j\in\mathcal{N}} V_{j,t,\omega} (G_{ij} \sin\theta_{ij,t,\omega} - B_{ij} \cos\theta_{ij,t,\omega}) \quad (7)$$

Voltage and line-flow limits:

$$V^{\min} \leq V_{i,t,\omega} \leq V^{\max}, \forall i,t,\omega \quad (8)$$

$$-F_{ij}^{\max} \leq F_{ij,t,\omega} \leq F_{ij}^{\max}, \forall (i,j) \in \mathcal{L}, t, \omega \quad (9)$$

For the IEEE 69-bus results reported in this paper, branch flows, voltage magnitudes, and voltage-security headroom are evaluated using the full nonlinear AC nodal active- and reactive-power balance in Eqs. (6)–(7). No LinDistFlow or other linearized feeder model is used for the reported benchmark values; line-flow and voltage limits are enforced within the same AC-feasibility model. The voltage-security headroom at each time and scenario is the minimum distance of the bus-voltage profile to the admissible lower or upper voltage limits:

$$h_{t,\omega} \leq V_{i,t,\omega} - V^{\min}, \forall i,t,\omega \quad (10)$$

$$h_{t,\omega} \leq V^{\max} - V_{i,t,\omega}, \forall i,t,\omega \quad (11)$$

$$h_{t,\omega} \geq 0, \forall t,\omega \quad (12)$$

Scenario energy not served and expected energy not served:

$$ENS_\omega = \sum_{t\in\mathcal{T}} \sum_{i\in\mathcal{N}} ls_{i,t,\omega} \Delta t, EENS = \sum_{\omega\in\Omega} \pi_\omega ENS_\omega; ls_{i,t,\omega} \geq 0 \quad (13)$$

The curtailment variable $ls_{i,t,\omega}$ represents involuntary unserved demand and is distinct from the voluntary DSM adjustment $u_{i,t,\omega}$. Consequently, ENS/EENS counts only energy that cannot be served under the modeled network, resource, and device constraints; price-responsive load shifting or voluntary demand reduction is not counted as unserved energy. The aggregate EENS values reported below are not disaggregated by initiating contingency in the present validation.

Generator and storage operating limits and dynamics:

$$0 \leq p_{g,t,\omega} \leq P_g^{\max}, -Q_g^{\max} \leq q_{g,t,\omega} \leq Q_g^{\max}, \forall g,t,\omega \quad (14)$$

$$0 \leq p_{s,t,\omega}^{\mathrm{ch}} \leq z_s P_s, 0 \leq p_{s,t,\omega}^{\mathrm{dis}} \leq z_s P_s, \forall s,t,\omega \quad (15)$$

$$\mathrm{SoC}_{s,t+1,\omega} = \mathrm{SoC}_{s,t,\omega} + \eta_s^{\mathrm{ch}} p_{s,t,\omega}^{\mathrm{ch}} \Delta t - \frac{1}{\eta_s^{\mathrm{dis}}} p_{s,t,\omega}^{\mathrm{dis}} \Delta t, \forall s,t,\omega \quad (16)$$

$$0 \leq \mathrm{SoC}_{s,t,\omega} \leq z_s E_s, \mathrm{SoC}_{s,T,\omega} = \mathrm{SoC}_{s,0,\omega}, \forall s,t,\omega \quad (17)$$

$$p_{s,t,\omega}^{\mathrm{ch}} p_{s,t,\omega}^{\mathrm{dis}} = 0, \forall s,t,\omega \quad (18)$$

The DES degradation term used in SWI is an operational throughput-cost surrogate. Depth-of-discharge-dependent aging, temperature-dependent degradation, capacity fade, and state-of-health evolution are not represented explicitly; consequently, the formulation evaluates short-horizon operating degradation cost rather than lifetime battery replacement economics.

Demand-response bounds and optional energy-neutrality:

$$-u_{i,t}^{\max} \leq u_{i,t,\omega} \leq u_{i,t}^{\max}, \forall i,t,\omega \quad (19)$$

$$\sum_{t\in\mathcal{T}} u_{i,t,\omega} \Delta t \in [-R_i, R_i], \forall i,\omega \quad (20)$$

DSM is represented as an aggregate bus-level flexible-load adjustment with time-dependent up/down bounds, availability, and optional horizon energy neutrality. The quadratic utility captures the economic value of served demand, but the formulation does not model appliance-level comfort, minimum on/off durations, heterogeneous customer participation, rebound dynamics, or a separate aggregator market-clearing layer. The DSM results should therefore be interpreted as system-level flexibility within prescribed participation bounds rather than as a detailed behavioral model of individual customers.

The realized demand $d_{i,t,\omega} = d_{i,t,\omega}^f + u_{i,t,\omega}$ enters (6). The planning-operation linkage for siting/sizing, with an optional cap K on installed sites, is:

$$E_s \leq z_s E_s^{\max}, P_s \leq z_s P_s^{\max}, z_s \in \{0,1\}, \forall s \in \mathcal{S} \quad (21)$$

$$\sum_{s\in\mathcal{S}} z_s \leq K \quad (22)$$

Solution use. The first stage selects $(z_s, E_s, P_s)_{s\in\mathcal{S}}$ offline. With these decisions fixed, the operational problem (5)–(20) is solved over a moving horizon using updated load, renewable, price, and DR-availability forecasts. The Pareto frontier is generated by sweeping the

weights of the normalized objectives or by epsilon constraints. Because SWI, SOI, and the technical penalty are normalized before scalarization, the weights express preferences rather than units. Equal weights are reported only as one reference setting and are not treated as universally optimal. Accordingly, "online" and "real-time" in this manuscript refer to completion of the receding-horizon scheduling problem within the one-hour control interval; they do not imply millisecond control or transient stabilization.

3. Multi-objective Co-optimization Framework

This section writes the joint problem as a two-stage, scenario-based, multi-period program. First-stage variables $x = \{z_s, E_s, P_s\}_{s\in\mathcal{S}}$ are chosen before uncertainty is realized. Second-stage variables

$y_\omega = \{p_{g,t,\omega}, q_{g,t,\omega}, V_{i,t,\omega}, \theta_{i,t,\omega}, p^{\mathrm{ch}}_{s,t,\omega}, p^{\mathrm{dis}}_{s,t,\omega}, \mathrm{SoC}_{s,t,\omega}, u_{i,t,\omega}, ls_{i,t,\omega}\}$ adapt to time t and scenario ω. The objectives depend on (x, y) as follows:

$$\max\left[\mathrm{SWI}^N(x,y), \mathrm{SOI}(x,y), TI(x,y)\right] \quad (23)$$

Weighted-sum Pareto generation uses normalized objectives and nonnegative preference weights:

$$J(w) = w_1\mathrm{SWI}^N + w_2\mathrm{SOI} + w_3 TI, w_k \geq 0, \sum_{k=1}^{3} w_k = 1 (24)$$

Epsilon-constraint alternative for scale-independent Pareto tracing:

$$\max \mathrm{SWI}^N(x,y) \mathrm{s.t.} \mathrm{SOI}(x,y) \geq \sigma, TI(x,y) \geq \tau \quad (25)$$

Here σ and τ are target levels used to trace the Pareto frontier. The two-stage scenario-recourse form is:

$$\max_{x\in X} \mathbb{E}_\omega[\Phi(x;\omega)], \Phi(x;\omega) = \max_{y_\omega \in Y(x,\omega)} J_\omega(w; x, y_\omega) \quad (26)$$

The set X contains the siting/sizing and investment constraints, and $Y(x,\omega)$ contains the operational constraints for fixed x. The scenario function J_ω is evaluated with the same AC-network limits used in the final feasibility check. The planning layer is mixed-integer and computationally demanding; fixing x in the operational layer removes the siting integers, permits warm starts, and substantially reduces the online problem. Large systems can use decomposition or convex network relaxations, followed by an AC feasibility check.

$$y^{\mathrm{opt}}_{t:t+H-1} = \mathrm{RHC}\left(d^f, p^{r,f}, \lambda, \rho^{\mathrm{DR}}\right)_{t:t+H-1} \quad (27)$$

Equation (27) is executed at each control step while honoring the installed first-stage decisions. Load, renewable, price, and DSM-availability forecasts are updated over the horizon; the first action is applied and the problem is then re-solved. A solution is considered operationally feasible only when network/device constraints are satisfied and the solve time remains below the control interval. The present case uses an hourly interval and therefore demonstrates online scheduling and corrective coordination, not sub-second transient control. Optimal placement and online co-management operate on distinct time scales. Stage 1 is an offline siting/sizing problem solved once per planning horizon, whereas Stage 2 is a receding-horizon controller that updates storage set-points and DSM actions while locations and ratings remain fixed. The finite scenario set represents load, renewable, real-time-price, contingency, and DR-availability uncertainty, with each scenario weighted by its probability. Scenario recourse and forecast updates therefore provide scenario-based stochastic coordination; they do not constitute a distributionally robust or out-of-sample statistical guarantee.

4. Results and Discussion

Results are reported in two complementary layers. Tables 2–3 and Figs. 2–6 retain the reference operating-point analysis used for the controlled benchmark comparison. A separate reconstruction-based robustness extension evaluates a fixed 10-scenario ensemble on the reconstructed feeder data basis and is used to quantify scenario dispersion, parameter sensitivity, and computational feasibility. The two result layers are therefore interpreted within their respective data and normalization contexts rather than treated as numerically interchangeable.

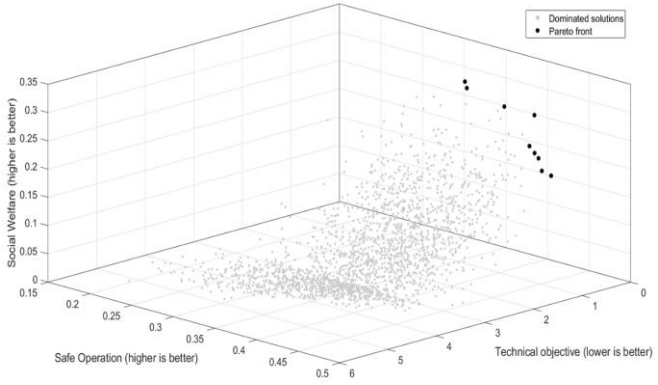

Fig. 2. Candidate solutions and non-dominated Pareto front; the selected knee solution is identified.

In this study, the proposed framework is tested on the IEEE 69-bus radial distribution feeder using an AC power-flow model with hourly resolution over a 24-hour horizon. Inputs comprise per-bus active/reactive load profiles, an exogenous real-time price signal, voltage and thermal limits, a set of candidate storage locations along main and lateral feeders, storage efficiencies and power/energy limits with state-of-charge dynamics, and bounded up/down demand response with optional daily energy neutrality. Performance is assessed using the three indices defined earlier: Social Welfare Index (consumer utility minus operating/degradation costs), Safe Operating Index (blend of voltage headroom and expected energy not served), and a technical metric capturing losses and voltage deviation. In Figure 2, the 3D Pareto surface reveals clear trade-offs: points near the technical extreme minimize losses/voltage deviation at the expense of smaller welfare gains, while points near the welfare extreme increase consumer surplus with slightly tighter security margins. A knee region emerges where modest compromises in one objective unlock large improvements in the others; subsequent time-series analyses use solutions from this knee for a balanced operating point. As reported in Table 2, optimal storage units concentrate at electrically stressed locations (e.g., buses 11, 21, and 50) with feeder-appropriate capacities, while optimal load reductions appear at downstream buses with pronounced peaks or weak headroom (e.g., buses 19, 27, and 61). This spatial pattern co-locates storage to relieve branch loading and support voltages and targets demand reductions where local peaks originate, producing complementary benefits that storage-only or DR-only baselines cannot achieve. The validation uses a balanced single-feeder representation; consequently, the reported numerical conclusions are restricted to the IEEE 69-bus system and are not generalized to unbalanced or multi-feeder networks. The controlled benchmark configurations in Table 3 use the same reference feeder data, 24-hour active/reactive-load and price trajectories, DES/DSM limits, objective normalization, and AC-feasibility checks. Figures 3–6 correspond to this reference operating-point comparison. The separate 10-scenario reconstruction-based robustness analysis is reported in Section 4.1 and is used for scenario dispersion and sensitivity rather than to redefine the reference curves.

Figure 2 uses consistent objective directions: the technical penalty is lower-is-better, whereas SOI and SWI are higher-is-better. Gray markers represent dominated candidates, black markers form the non-dominated Pareto front, and the annotated knee is the balanced solution used in Table 2 and the hourly comparisons. The knee is selected from normalized objectives, so its identification is independent of the physical units of welfare, EENS, losses, and voltage deviation.

Table 2. Optimal placement of energy storage and load reduction in IEEE 69-bus system.

Optimal Bus (Storage)	Optimal Capacity (kWh)	Optimal Bus (Load Reduction)	Optimal Load Reduction (kW)
11	1450	19	220
21	1300	27	180
50	950	61	150

Figure 3 shows peak shaving and mild valley filling at the selected Pareto-knee operating point, with the daily energy difference remaining small relative to the original profile. The lower peak and smoother ramps reduce the loading conditions associated with feeder losses and voltage deviation.

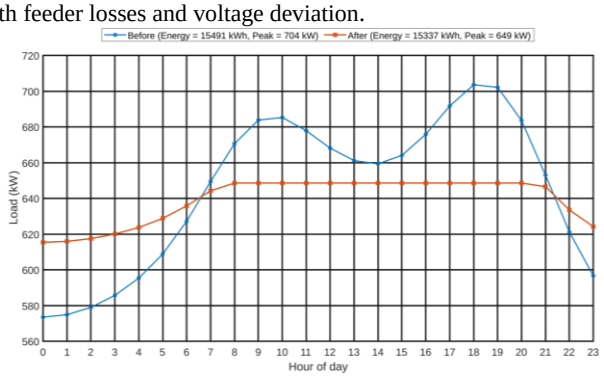

Fig. 3. Load curve before and after optimal placement over 24 hours.

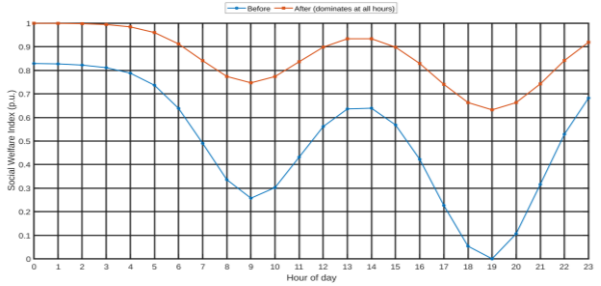

Fig. 4. Social Welfare Index before and after optimal placement over 24 hours.

Figure 4 shows a higher SWI at each plotted hour of the probability-weighted expected trajectory, reflecting load shifting away from expensive periods together with lower effective supply costs. Figure 5 shows the corresponding expected SOI trajectory, for which increased voltage headroom and lower involuntary curtailment improve the composite index. Figure 6 shows the expected Technical Index obtained from the normalized loss and voltage-deviation penalty. These plots are probability-weighted expected trajectories from the scenario-recourse model and should not be interpreted as worst-case contingency traces. Within this selected operating point, the siting decisions in Table 2 and the coordinated DES-DSM actions provide complementary technical, security, and welfare benefits on the IEEE 69-bus feeder.

The daily energy difference between the two load profiles is 154 kWh, corresponding to 0.99% of the original daily energy, while the peak decreases from 704 to 649 kW.

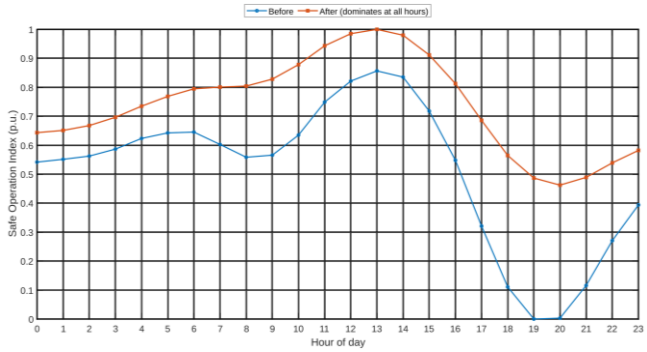

Fig. 5. Safe Operating Index before and after optimal placement over 24 hours.

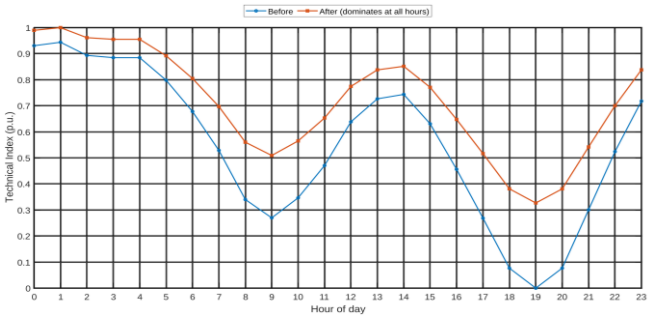

Fig. 6. Technical Index before and after optimal placement over 24 hours.

The comparative results in Table 3 evaluate the proposed method against four controlled, reference-informed benchmark configurations: DES-DSM coordination with storage locations fixed a priori, DES siting with DSM disabled, welfare-focused DSM without optimized storage siting, and stability-oriented active-reactive coordination without DSM. Each benchmark is implemented on the same IEEE 69-bus model by fixing or disabling the corresponding planning or operational capability while retaining common input profiles, DES/DSM limits, objective normalization, and AC-feasibility screens. The citations in the benchmark labels identify the methodological feature motivating each configuration; the table does not claim to reproduce the original authors' numerical implementations or test systems. Under these common conditions, the proposed formulation attains the highest values of the three reported normalized indices, the largest feeder-loss and peak reductions, and the lowest EENS among the evaluated configurations.

Table 3. Performance comparison with controlled reference-informed benchmark configurations on the same IEEE 69-bus test system.

Method	Load reduction (%)	Social Welfare Index (p.u.)	Safe Operating Index (p.u.)	Technical Index (p.u.)	Feeder-loss reduction (%)	Avg. min. voltage headroom (p.u.)	EENS (MWh)	Peak-demand reduction (%)
Fixed-site DES–DSM [1]	4.1	0.76	0.72	0.70	7.3	0.014	0.12	6.1
DES siting only [2]	0.0	0.70	0.75	0.78	12.1	0.018	0.09	0.0
Welfare-focused DSM [6]	6.0	0.82	0.70	0.68	5.5	0.013	0.15	8.0
Stability-oriented control [16]	0.0	0.74	0.78	0.80	10.2	0.017	0.08	0.0
Proposed method	8.7	0.92	0.90	0.88	17.8	0.026	0.02	12.5

Note: All benchmark configurations are implemented on the same IEEE 69-bus feeder with identical input profiles, DES/DSM limits, objective normalization, and AC-feasibility checks. They are controlled model variants, not direct numerical reproductions of the cited papers.

The comparison also explains the source of the improvement. Methods without optimized siting leave electrical bottlenecks insufficiently supported; siting-only methods cannot exploit price-driven load flexibility; welfare-only DSM can increase customer value while overlooking local network stress; and stability-oriented coordination without DSM cannot shift demand away from high-price, high-stress periods. The proposed architecture combines these effects by locating storage at high-value buses and coordinating storage and DSM online. This interpretation is restricted to the evaluated benchmark cases in Table 3. Table 3 reports EENS = 0.02 MWh for the reference benchmark setting. In the separate fixed 10-scenario reconstruction, voluntary price-responsive DSM is distinguished from involuntary curtailment and no involuntary ENS occurs, giving EENS = 0 for that auxiliary ensemble. The two EENS values arise from distinct validation settings and are not pooled; EENS is compared only within a common setting. The operating-point ranking in Table 3 remains conditional on the selected reference data, normalization, and preference parameters. The reconstruction-based sensitivity study therefore examines the SOI mixing coefficient α, objective preferences, and demand-price elasticity without treating the original ranking as parameter-invariant.

4.1. Scenario Dispersion, Sensitivity, and Computational Validation

A fixed ensemble of 10 equiprobable scenarios is evaluated with a fixed random seed to represent uncertainty in load, renewable availability, real-time price, contingency state, and DR availability. Table 4 reports the mean, standard deviation, minimum, and maximum of the principal reconstructed indices. Figure 7 summarizes sensitivity to the SOI mixing coefficient, representative objective-preference settings, and demand-price elasticity. The reconstructed IEEE 69-bus analysis is an auxiliary robustness check; its absolute load and loss quantities are interpreted within the reconstructed data basis rather than compared directly with the reference operating-point values in Figs. 3–6 and Table 3.

Table 4. Scenario dispersion in the reconstructed IEEE 69-bus robustness analysis.

Metric	Mean	SD	Min	Max
SWI	0.6596	0.0411	0.5890	0.7311
SOI	0.8057	0.0566	0.6863	0.8802
Technical Index	0.2144	0.0120	0.1908	0.2317
EENS (MWh)	0.0000	0.0000	0.0000	0.0000
Voltage headroom (Pu)	0.0306	0.0057	0.0186	0.0380
Feeder losses (kWh)	3309.0143	611.8981	2485.0260	4592.3550
Peak demand (kW)	3874.5963	328.2311	3452.2652	4505.1502
Peak reduction (%)	8.0100	1.2889	5.8732	10.0000

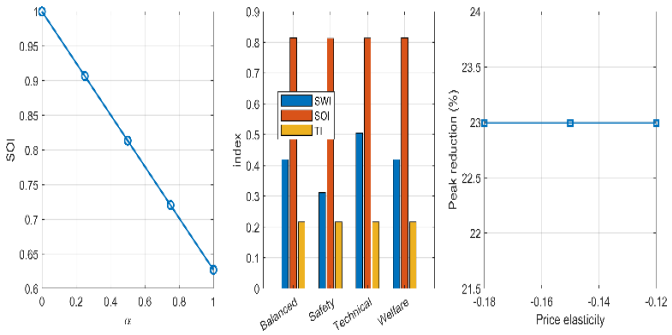

Fig. 7. Sensitivity of reconstructed validation metrics to (a) the SOI mixing coefficient α, (b) objective preference weights, and (c) demand-price elasticity.

Figure 7 shows a clear dependence of the composite SOI on α, while the representative objective-weight settings redistribute the normalized performance indices without eliminating the underlying trade-off. The tested elasticity range produces comparatively limited variation in the reported peak-reduction response. These results support a parameter-dependent interpretation and do not imply invariance to weighting or elasticity choices. The reconstruction-based calculations were executed in MATLAB R2024b with nonlinear radial AC power-flow feasibility checks. The 10-scenario IEEE 69-bus study records a mean Stage-2 operational solve time of 0.140 s and a maximum of 0.248 s. These wall-clock values support only the stated one-hour scheduling interval; Stage 1 remains an offline planning task and is not used to justify real-time execution. Table 5 provides the corresponding second-feeder execution summary for the IEEE 33-bus case.

Table 5. Stage-2 operational timing and second-feeder execution summary.

Network	Stage-2 mean (s)	Stage-2 max (s)	SWI mean	Scenarios
IEEE 69-bus	0.1401	0.2484	0.6596	10
IEEE 33-bus	0.0146	0.0158	0.6596	10

The IEEE 33-bus case is used as a compact cross-network execution and feasibility check under the same reconstructed economic-index definitions and 10-scenario protocol. The identical reported SWI means are not interpreted as identical electrical-network performance; network transferability remains bounded by the limited metrics reported for the second feeder.

5. Conclusions

This paper presents a two-stage co-optimization framework linking DES siting/sizing with hourly DSM coordination under real-time pricing. The reference operating-point analysis retains the controlled benchmark comparison, while a separate reconstructed 10-scenario assessment quantifies dispersion and sensitivity to the SOI mixing coefficient, objective preferences, and demand-price elasticity. The Stage-2 execution times remain well below the one-hour scheduling interval in the reconstructed IEEE 69-bus study, and the IEEE 33-bus case provides a compact second-feeder execution and feasibility check. These results support the formulation within the evaluated feeders, data bases, normalization choices, and uncertainty settings; they do not establish parameter-invariant or universal superiority. The remaining limitations include aggregate price-responsive DSM, throughput-based battery degradation without lifetime/SoH dynamics, limited second-feeder performance metrics, and the absence of unbalanced-feeder, hardware-in-the-loop, and field validation.

References

[1] X. Zhang, Y. Son, and S. Choi, "Optimal scheduling of battery energy storage systems and demand response for distribution systems with high penetration of renewable energy sources," *Energies*, vol. 15, 2022.

[2] R. Su et al., "Optimal placement and capacity sizing of energy storage systems via NSGA-II in active distribution network," *Front. Energy Res*., vol. 10, 2023.

[3] C. H. B. Apribowo, S. P. Hadi, F. D. Wijaya, and M. I. B. Setyonegoro, "Optimal sizing and placement of battery energy storage system for maximum variable renewable energy penetration considering demand response flexibility: A case in Lombok power system, Indonesia," *Energy Convers. Manag.: X*, vol. 23, 2024.

[4] M. Asadi, S. M. Abedi, and H. Siahkali, "Providing an optimal demand response program through placement of automatic switches and energy storage systems to improve the reliability of power distribution networks," *IET Gener. Transm. Distrib.*, vol. 17, pp. 2115-2129, 2023.

[5] M. A. El-Meligy, M. Sharaf, and K. A. Alnowibet, "Voltage stability-constrained robust transmission expansion planning using binary discretization technique," *Electr. Power Syst. Res.*, vol. 231, 2024.
[6] F. Moazzen, M. Alikhani, J. Aghaei, and M. Hossain, "Social welfare evaluation during demand response programs execution considering machine learning-based load profile clustering," *Appl. Energy*, vol. 357, 2024.
[7] C. Li et al., "Optimal allocation of multi-type FACTS devices in power systems based on power flow entropy," *J. Mod. Power Syst. Clean Energy*, vol. 2, pp. 173-180, 2014.
[8] Y. Weng, Y. Liu, R. L. T. Lim, and H. D. Nguyen, "Distributed energy resource exploitation through co-optimization of power system and data centers with uncertainties during demand response," *Sustainability*, vol. 15, 2023.
[9] V. Amir, "Optimal distributed generation and capacitor placement in power distribution networks for power-loss minimization with the bat algorithm," *Majlesi J. Energy Manag.*, vol. 12, pp. 20-27, 2023.
[10] M. H. Ranjbari, R. Dalili, and M. Pishvaei, "An analytical approach for optimal placement and sizing of energy storage," *Majlesi J. Energy Manag.*, vol. 6, 2017.
[11] A. Moghtadaei and M. H. Vafaee, "Optimal multi-objective placement and sizing of multiple DGs and DSTATCOMs via MOPSO," *Majlesi J. Energy Manag.*, vol. 6, pp. 35-40, 2017.
[12] S. J. A.-D. Hosseini, M. Moazzami, and H. Shahinzadeh, "Optimal sizing of an isolated hybrid wind/PV/battery system considering loss-of-power-supply probability," *Majlesi J. Electr. Eng.*, vol. 11, pp. 63-69, 2017.
[13] W. K. Al-Azzawi et al., "Economic optimization of a wind, solar, and battery-storage combination for grid-independent power supply using the cuckoo optimization algorithm," *Majlesi J. Electr. Eng.*, vol. 17, pp. 19-25, 2023.
[14] D. Wang, R. Fan, P. Yang, K. Du, X. Xu, and R. Chen, "Research on floating real-time pricing strategy for microgrid operator in local energy market considering shared energy storage leasing," *Appl. Energy*, vol. 368, 2024.
[15] M. D. Furió Ortega and J. Moreno del Castillo, "Dynamic demand response to electricity prices: Evidence from the Spanish retail market," *Utilities Policy*, 2024.
[16] X. Wang et al., "Multi-objective coordinated optimization method of active and reactive power considering power characteristics of renewable energy converters," *Energies*, vol. 17, 2024.
[17] E. Priya, and P. Roselyn J, "An integrated approach for multi-objective differential algorithm-based event-constrained optimal power flow for power-system resiliency enhancement," *Sustain. Resilient Infrastruct.*, vol. 10, pp. 351-370, 2025.
[18] H. Zakernezhad, M. Setayesh Nazar, M. Shafie-khah, and J. P. S. Catalão, "Optimal scheduling of an active distribution system considering distributed energy resources, demand response aggregators and electrical energy storage," *Appl. Energy*, vol. 314, 2022.
[19] A. Najafi-Ghalelou, M. Khorasany, and R. Razzaghi, "Maximizing social welfare of prosumers in neighborhood battery-enabled distribution networks," *Appl. Energy*, vol. 359, 2024.
[20] A. Zarei, N. Ghaffarzadeh, and F. Shahnia, "Optimal demand response scheduling and voltage reinforcement in distribution grids incorporating uncertainties of energy resources, placement of energy storages, and aggregated flexible loads," *Front. Energy Res.*, vol. 12, 2024.